Estimation of the Hydrophobic Effect in an Antigen−Antibody Protein−Protein Interface[†,‡]

Eric J. Sundberg,[§] Mariela Urrutia,[§,||] Bradford C. Braden,[§,⊥] Jordi Isern,[§] Daisuke Tsuchiya,[§,#] Barry A. Fields,[§,○] Emilio L. Malchiodi,[||] José Tormo,[§,▽] Frederick P. Schwarz,[§] and Roy A. Mariuzza*[,§]

Center for Advanced Research in Biotechnology, University of Maryland Biotechnology Institute and National Institute of Standards and Technology, 9600 Gudelsky Drive, Rockville, Maryland 20850, Bowie State University, Bowie, Maryland 20715, and Instituto des Estudios de la Inmunidad Humoral, CONICET, Catedra de Inmunologia, FFyB, UBA, Junin 959, 1113 Buenos Aires, Argentina

Received March 28, 2000; Revised Manuscript Received October 17, 2000

ABSTRACT: Antigen−antibody complexes provide useful models for analyzing the thermodynamics of protein−protein association reactions. We have employed site-directed mutagenesis, X-ray crystallography, and isothermal titration calorimetry to investigate the role of hydrophobic interactions in stabilizing the complex between the Fv fragment of the anti-hen egg white lysozyme (HEL) antibody D1.3 and HEL. Crystal structures of six FvD1.3−HEL mutant complexes in which an interface tryptophan residue (V_LW92) has been replaced by residues with smaller side chains (alanine, serine, valine, aspartate, histidine, and phenylalanine) were determined to resolutions between 1.75 and 2.00 Å. In the wild-type complex, V_LW92 occupies a large hydrophobic pocket on the surface of HEL and constitutes an energetic "hot spot" for antigen binding. The losses in apolar buried surface area in the mutant complexes, relative to wild-type, range from 25 (V_LF92) to 115 Å^2 (V_LA92), with no significant shifts in the positions of protein atoms at the mutation site for any of the complexes except V_LA92, where there is a peptide flip. The affinities of the mutant Fv fragments for HEL are 10−100-fold lower than that of the original antibody. Formation of all six mutant complexes is marked by a decrease in binding enthalpy that exceeds the decrease in binding free energy, such that the loss in enthalpy is partly offset by a compensating gain in entropy. No correlation was observed between decreases in apolar, polar, or aggregate (sum of the apolar and polar) buried surface area in the V_L92 mutant series and changes in the enthalpy of formation. Conversely, there exist linear correlations between losses of apolar buried surface and decreases in binding free energy ($R^2 = 0.937$) as well as increases in the solvent portion of the entropy of binding ($R^2 = 0.909$). The correlation between binding free energy and apolar buried surface area corresponds to 21 cal mol^{-1} Å^{-2} (1 cal = 4.185 J) for the effective hydrophobicity at the V_L92 mutation site. Furthermore, the slope of the line defined by the correlation between changes in binding free energy and solvent entropy approaches unity, demonstrating that the exclusion of solvent from the binding interface is the predominant energetic factor in the formation of this protein complex. Our estimate of the hydrophobic contribution to binding at site V_L92 in the D1.3−HEL interface is consistent with values for the hydrophobic effect derived from classical hydrocarbon solubility models. We also show how residue V_LW92 can contribute significantly less to stabilization when buried in a more polar pocket, illustrating the dependence of the hydrophobic effect on local environment at different sites in a protein−protein interface.

It is widely accepted that the hydrophobic effect provides the driving force for protein folding (*1*). Hydrophobic interactions are also believed to play an essential role in stabilizing protein−protein complexes (*2*−*6*), whose interfaces are frequently, though not always, composed of a cluster of "hot spot" residues at the center of the interface surrounded by energetically less important residues that serve largely to exclude bulk solvent from the hot spots (*5*, *6*). Because of its importance in protein folding and protein−protein association, numerous attempts have been made to estimate the magnitude of the hydrophobic effect using a variety of approaches. Early model studies provided evidence for a linear relationship between the free energy of transfer of small hydrophobic solutes from aqueous to hydrophobic solvents and the burial of solvent-accessible hydrophobic surface area, with constants of proportionality ranging from 20 to 30 cal mol^{-1} Å^{-2} (*7*−*11*). With the advent of protein engineering techniques, it became possible to substitute a hydrophobic residue within the core of a protein by a smaller

[†] This work was supported by NIH Grant GM52801.

[‡] Atomic coordinates have been deposited in the Brookhaven Data Bank as entries 1G7H, 1G7I, 1G7J, 1G7L, and 1G7M.

* To whom correspondence should be addressed. Telephone: (301)-738-6243. Fax: (301)738-6255. E-mail: mariuzza@carb.nist.gov.

[§] Center for Advanced Research in Biotechnology.

[||] Instituto des Estudios de la Inmunidad Humoral.

[⊥] Bowie State University.

[#] Present address: Biomolecular Research Engineering Institute, 6-2-3 Furuedai, Suita, Osaka 565-0874, Japan.

[○] Present address: Department of Biochemistry, University of Sydney, New South Wales 2006, Australia.

[▽] Present address: Centro Nacional de Biotecnologia C.S.I.C., Campus de la Universidad Autonoma de Madrid, Cantoblanco 28049, Madrid, Spain.

10.1021/bi000704l CCC: $19.00
Published on Web 11/22/2000

hydrophobic residue and, by measuring the resulting change in stability of the folded state as compared to the unfolded state ($\Delta\Delta G_{unfolding}$), to estimate the difference between the hydrophobic stabilization provided by the two amino acids. In these experiments, the observed decreases in stability are generally greater than predicted from solvent transfer scales, up to 80 cal mol^{-1} Å^{-2} (*12*−*19*). However, a serious difficulty in interpreting the effects of large-to-small substitutions within protein cores is that such mutations generally create cavities, resulting in the loss of favorable van der Waals contacts between the bulky side chain removed and the atoms that form the walls of the cavity. For T4 lysozyme, a correlation was found between $\Delta\Delta G_{unfolding}$ and cavity size for a series of leucine-to-alanine substitutions at different sites in the protein core (*16*, *19*). The overall decrease in stability could be deconvoluted into two terms: one associated with cavity volume, which is presumably due to the loss of van der Waals interactions, and a constant term close in value to the transfer free energy of leucine relative to alanine, as determined by partitioning between water and organic solvents. For barnase, however, no correlation between $\Delta\Delta G_{unfolding}$ and cavity volume was apparent for isoleucine-to-valine mutants (*20*), although an approximately linear relationship between these parameters was noted for isoleucine-to-alanine mutants (*21*). In a series of valine-to-alanine mutants of human lysozyme, there was no correlation between $\Delta\Delta G_{unfolding}$ and cavity volume, or between $\Delta\Delta G_{unfolding}$ and changes in the hydrophobic surface area exposed upon denaturation (*18*). It is therefore apparent that extracting hydrophobic free energies from the effects on stability of large-to-small substitutions in protein cores is not a straightforward task, most likely due to secondary effects associated with the substitutions, including loss of van der Waals contacts at the mutation site and structural adjustments in the protein as nearby atoms shift toward the space vacated by the wild-type side chain.

In the present study, we describe a different, and potentially simpler, approach to measuring the hydrophobic effect in proteins that relies on correlating changes in buried surface area in a protein−protein complex upon mutation of a large hydrophobic interface residue with changes in the binding free energy. As a model, we used the complex between the Fv[1] fragment (a heterodimer consisting of only the light and heavy chain variable domains, V_L and V_H) of the anti-hen egg white lysozyme (HEL) D1.3 antibody and HEL. The crystal structure of the FvD1.3−HEL complex is known to high resolution (1.8 Å) (*22*), and alanine scanning mutagenesis has been carried out to map the binding energetics in the interface (*23*, *24*). These studies have revealed that only 3 of 14 D1.3 contact residues (V_LW92, V_HD100, and V_HY101) are responsible for the majority of binding energy associated with complex formation, with each mutation resulting in a $\Delta\Delta G_b > 2.5$ kcal/mol. More moderate but still significant effects were seen for substitutions at V_LY32 and V_HE98 ($\Delta\Delta G_b = 1.0-2.0$ kcal/mol), while mutations at nine other contact residues contributed insignificantly to the binding energy ($\Delta\Delta G_b < 1.0$ kcal/mol). We chose the V_LW92 hot spot for measuring the hydrophobic contribution to binding because it is a large nonpolar residue that, unlike V_HY101, is partly solvent-exposed in the D1.3−HEL interface. We reasoned that the lower packing density of a partly buried interface residue as compared to one that is completely buried should minimize the van der Waals component of the binding interaction, permitting the hydrophobic term to dominate. In addition, the loss of protein−protein van der Waals contacts at a solvent-accessible site should be compensated, at least in part, by rearrangements in solvent structure that restore shape complementarity between the interacting surfaces, as previously described (*24*−*26*).

By determining the high-resolution crystal structures of six FvD1.3−HEL complexes with large-to-small substitutions at hot spot position V_L92 and measuring their affinities by titration calorimetry, we show that there are linear relationships between the loss of apolar buried surface area and the decrease in binding free energy as well as the increase in the solvent portion of the binding entropy in the mutant complexes. Notably, there exist no correlations between the apolar, polar, or aggregate (sum of apolar and polar) buried surface areas and changes in the enthalpy of formation. We estimate the effective hydrophobicity at site V_L92 of D1.3 to be 21 cal mol^{-1} Å^{-2} and find that this change in free energy is accounted for predominantly by relative gains in the solvent entropy upon complex formation. This value falls within the range of transfer free energies per unit of buried hydrophobic surface area determined for small apolar solutes (*7*−*11*). By comparing crystal structures and thermodynamic data of D1.3 binding to HEL and its anti-idiotypic antibody E5.2, we also show that residue D1.3 V_LW92 contributes considerably less to binding if packed against a more polar surface than in the D1.3−HEL complex, emphasizing the importance of local environment in determining the magnitude of the hydrophobic effect at individual sites in a protein−protein interface.

EXPERIMENTAL PROCEDURES

Production of Fv Fragments. The monoclonal anti-HEL antibody D1.3 derives from a Balb/c mouse hyperimmunized with HEL (*27*). The FvD1.3 and the mutants were prepared from the culture supernatants of recombinant *Escherichia coli* BMH 71−18 cells (*28*) transformed with the pUC19-based expression vector pSW1−VHD1.3−VKD1.3 (*29*). For protein production, recombinant clones were resuspended in 10 mL of Terrific broth (*30*) containing 100 μg/mL ampicillin and 1% (w/v) glucose. The cultures were incubated at 37 °C under agitation to an absorbance of 1.0 at 600 nm. The cells were then pelleted by centrifugation and resuspended in 500 mL of Terrific broth containing 100 μg/mL ampicillin and 0.2% (w/v) glucose. The cultures were grown at 37 °C to an absorbance of 1.0, and isopropyl-β-D-thiogalactoside (Gold Biotechnology, St. Louis, MO) was added to a final concentration of 0.2 mM. After further incubation at 37 °C for 4 h, the bacteria were pelleted, and FvD1.3 was affinity purified from the supernatant using the anti-D1.3 monoclonal antibody E5.2 (*31*) coupled to Sepharose columns. Columns were washed with 100 volumes of phosphate-buffered saline (PBS) with 0.65 M final NaCl concentration, pH 7.4, and eluted with 50 mM diethylamine, pH 12. Fractions were immediately neutralized with 1.0 M Tris-HCl, pH 7.0, and concentrated using Centricon 3000 spin columns (Amicon,

[1] Abbreviations: HEL, hen egg white lysozyme; PBS, phosphate-buffered saline; V_L, light chain variable region; V_H, heavy chain variable region; Fv, a heterodimer consisting of only the V_L and V_H domains. Standard one-letter amino acid codes have been used throughout the text.

Beverly, MA). Further purification of the FvD1.3 mutants was carried out by size exclusion chromatography on a ZORBAX GF-250 column (DuPont) in 0.2 M sodium phosphate buffer, pH 7.4 (*32*).

Site-Directed Mutagenesis. Mutagenesis of FvD13 was carried out with the Quick Change Site-Directed Mutagenesis Kit (Stratagene, La Jolla, CA). Mutagenic oligonucleotides were designed to replace the FvD1.3 W92 wild-type codon with that for alanine (GCT), aspartate (GAC), histidine (CAC), phenylalanine (TTC), serine (AGT), or valine (GTC). Prior to expression, all mutations were confirmed by the dideoxynucleotide sequencing method using a Sequenase Version 2.0 kit (USB, Cleveland, OH).

Measurement and Calculation of Thermodynamic Parameters. The interaction of soluble wild-type FvD1.3 with immobilized HEL was measured by surface plasmon resonance detection using a BIAcore 1000 biosensor (Pharmacia Biosensor, Uppsala, Sweden) as described (*23*). The data were analyzed using the BIAevaluation 2.1 software package (Pharmacia). The binding constant (K_b) for the wild-type reaction was determined from Scatchard analysis after correction for nonspecific binding, by measuring the concentration of free reactants and complex at equilibrium. Isothermal titration calorimetry was used to determine the enthalpic component of D1.3−HEL association. Affinity-purified FvD1.3 mutants and HEL were dialyzed against PBS prior to calorimetry. In a typical experiment, 10 μL aliquots of a 1.00 mM HEL solution were titrated into a 0.05 mM Fv solution at 24.0 °C, and the evolved heats were measured with a Microcal Omega titration calorimeter as described (*22*, *25*, *33*, *34*). The titrations were continued beyond saturation of the antibody combining sites to determine any heat contributions due to dilution of the HEL solution upon its addition to the antibody solution. The heats below the saturation point were corrected accordingly for any heat of dilution of the HEL solution. Protein concentrations were calculated using 1% extinction coefficients at 280 nm of 1.50, 1.34, and 2.62 for wild-type FvD1.3, FvD1.3 mutants, and HEL, respectively. The total heat was fitted via a least squares minimization method (*33*) to the total antigen concentration to determine the binding enthalpy, ΔH_b, and estimate K_b. The binding entropy contribution, $T\Delta S_b$, was calculated from $\Delta G_b = \Delta H_b - T\Delta S_b$, where $\Delta G_b = -RT \ln(K_b)$. The binding entropy can be divided into terms defining the conformational and solvent portions, where $\Delta S_b = \Delta S_{conformation} + \Delta S_{solvent}$. The solvent portion of the entropy of binding is proportional to the heat capacity (ΔC_p), which is a function of the apolar and polar changes in accessible surface areas (ΔASA) of the entire binding interface and was calculated using the following set of equations (*35*−*37*):

$$\Delta C_p = \Delta C_{p,\text{apolar}} + \Delta C_{p,\text{polar}}$$

where

$$\Delta C_{p,\text{apolar}} = (0.45 + (2.63 \times 10^{-4})(T - 25) - (4.2 \times 10^{-5})(T - 25)^2) \times \Delta\text{ASA}_{\text{apolar}}$$

$$\Delta C_{p,\text{polar}} = (-0.26 + (2.85 \times 10^{-4})(T - 25) - (4.31 \times 10^{-5})(T - 25)^2) \times \Delta\text{ASA}_{\text{polar}}$$

and

$$\Delta S_{\text{solvent}} = \Delta C_p \ln(T/T_S^*)$$

where $T_S^* = 112 \pm 6$ °C.

Crystallography. A small molar excess of HEL (Boehringer-Mannheim, Indianapolis, IN) was added to purified FvD1.3 mutants, and the complexes were crystallized in hanging drops by vapor diffusion. Crystallization conditions for the V_L92D (*25*), V_L92F, V_L92A, V_L92H, and V_L92S complexes were similar to those used for the wild-type FvD1.3−HEL complex (*32*): 15−18% (w/v) poly(ethylene glycol) 8000 (Sigma, St. Louis, MO) and 0.1 M potassium phosphate, pH 6.0−6.5. The V_L92V complex, however, crystallized in 14% (w/v) poly(ethylene glycol) 8000, 0.1 M sodium acetate, 0.05 M sodium cacodylate, pH 6.5. Macroseeding in hanging drops was used to obtain crystals with dimensions up to 0.4 mm × 0.2 mm × 0.1 mm. A rotating copper anode source was used for X-ray diffraction, and data were collected on a Siemens HI-STAR area detector for the V_L92A, V_L92D, and V_L92F complexes and on a 345-mm MarResearch image plate detector for the V_L92H, V_L92S, and V_L92V complexes. Crystals of the V_L92A, V_L92H, and V_L92S complexes were soaked in 16% (w/v) poly(ethylene glycol) 8000, 20% glycerol, and 0.1 M potassium phosphate, pH 6.5, prior to flash-cooling in liquid N_2; the V_L92D, V_L92F, and V_L92V complexes were measured at room temperature. Diffraction data for the V_L92A, V_L92D, and V_L92F complexes were reduced using XENGEN version 2.0 (*38*); data for the V_L92H, V_L92S, and V_L92V complexes were reduced with DENZO/SCALEPACK (*39*). All complexes crystallized isomorphously with the wild-type complex in space group *C*2. However, data reduction for the second set of complexes resulted in distinct *a* axis and β angle cell parameters relative to the first set. As seen in Table 1, the cell parameters of the second set of complexes, although different from the first set, are isomorphous to one another. This represents an alternative, yet analogous, way to describe the cell due to the parameter choices assigned by two different data reduction programs. The refinement of the V_L92D complex has been described previously (*25*). Refinement of the V_L92A and V_L92F complexes was performed in a similar way using X-PLOR (*40*) and the wild-type complex (PDB accession code 1VFB) with all water molecules deleted as a model. Molecular replacement using the same unsolvated wild-type complex as a model was performed using AMoRe (*41*) for the second set of complexes in order to orient the model appropriately in the altered cell. Refinement then proceeded identically for all of the mutant complexes, except that CNS (*42*) was used for the second set of complexes instead of X-PLOR (*40*). The first refinement step consisted of rigid-body refinement, in which each of the three polypeptide chains (V_L, V_H, and HEL) were treated as independent rigid units. Next, an $F_{o(\text{mutant})} - F_{c(\text{wild type})}$ difference electron density map was calculated and inspected in order to confirm the mutation using the program O (*43*). Refinement then consisted of (i) modeling the mutation into the electron density, (ii) an additional stage of rigid-body refinement, (iii) one stage of simulated annealing refinement with a starting temperature of 3000 K, and (iv) iterative cycles of positional refinement, temperature factor refinement, and model building of protein residues and

Table 1: Data Collection and Refinement Statistics for Wild-Type and Mutant FvD1.3−Lysozyme Complexes[a]

	V_LW92A	V_LW92F	V_LW92H	V_LW92S	V_LW92V
Data Collection					
space group	*C*2	*C*2	*C*2	*C*2	*C*2
cell dimensions					
a (Å)	128.05	128.27	123.02	121.63	123.67
b (Å)	60.42	59.15	59.12	59.06	60.40
c (Å)	56.16	56.08	56.17	55.86	56.79
β (deg)	119.26	119.28	113.96	113.59	114.25
temperature (K)	100	100	100	100	298
resolution limit (Å)	1.85	1.80	1.75	2.00	1.90
mosaicity (deg)			0.5	1.1	0.4
R_{merge} (%)[b]			4.1(29.9)	5.1(35.0)	5.4(30.8)
unique reflections	22.760	30,405	35,748	23,556	27,663
total observations			69,273	53,007	84,329
completeness (%)	98.8(54.8)	98.3(82.6)	95.7(91.8)	95.7(93.1)	91.7(87.0)
Refinement					
R_{free}[c]		24.76	22.85	24.03	22.56
R_{cryst}	20.3	18.28	19.74	20.70	19.41
protein					
residues	352	352	348	346	352
average *B* (Å^2)	30.0	20.7	21.9	26.9	29.6
water					
molecules	150	398	348	217	116
average *B* (Å^2)	40.5	35.3	33.0	33.1	38.0
rms deviations					
bonds (Å)	0.016	0.009	0.012	0.008	0.005
angles (deg)	2.013	1.631	1.698	1.528	1.267

[a] Values in parentheses correspond to the highest resolution shell: V_LW92A (1.91−1.85 Å), V_LW92F (1.86−1.80 Å), V_LW92H (1.79−1.75 Å), V_LW92V (1.94−1.90 Å, and V_LW92S (2.05−2.00 Å). [b] $R_{merge} = \Sigma|I - \langle I\rangle|/\Sigma\langle I\rangle$, where *I* is the observed intensity and $\langle I\rangle$ is the average intensity of multiple observations of symmetry-related reflections. [c] A portion of the overall reflections was set aside for R_{free} calculations: V_LW92F (7.1%); V_LW92H (9.3%); V_LW92V (9.2%); and V_LW92S (9.4%).

Table 2: Contacts of FvD1.3 Residue V_L92 with Hen Egg White Lysozyme Antigen Residues and Water

	V_L92wt	V_L921A[a]	V_L92D	V_L92F	V_L92H	V_L92S	V_L92V
			Gln121				
C^{δ}	$C^{\epsilon 3}$ (3.8)^2, $C^{\zeta 3}$ (4.0)						
$N^{\epsilon 2}$	$C^{\epsilon 3}$ (3.8)						
			Arg125				
C^{α}	$C^{\eta 2}$ (4.0)						
C^{δ}	$C^{\zeta 2}$ (4.0)	O (3.6)					
C^{γ}	$C^{\zeta 2}$ (3.9), $C^{\eta 2}$ (3.8)						
			Ile124				
$C^{\delta 1}$	$C^{\zeta 3}$ (4.1)						
			Water				
H_2O 758	O (2.9)		O (2.9)	O (2.7)	O (2.6)	O (2.6)	O (2.8)
H_2O 882	$C^{\zeta 2}$ (3.6), $C^{\eta 2}$ (3.6)						
H_2O 984	$C^{\eta 2}$ (3.7)						
H_2O 874		O (2.6), C^{β} (3.7)					
H_2O 990			$O^{\delta 2}$ (3.1)				
H_2O 991			$O^{\delta 2}$ (2.8)				
H_2O 388				$C^{\epsilon 2}$ (3.7)			
H_2O 423				C^{ζ} (3.3)			
H_2O 521				$C^{\delta 2}$ (3.7)			
H_2O 613				C^{ζ} (3.5), $C^{\epsilon 2}$ (3.7)			
H_2O 378					$C^{\epsilon 1}$ (3.7)		
H_2O 380					$N^{\delta 1}$ (2.7)		
H_2O 510					$C^{\epsilon 1}$ (3.5)		
H_2O 429						O^{γ} (2.9)	
H_2O 465						O^{γ} (2.9)	

[a] V_L92A has a peptide flip at residue V_L92A. [b] The numbers in parentheses are the contact distances (in Å). Maximum contact distances are (in Å) as follows: C−C, 4.1; C−N, 3.8; C−O, 3.7; O−O, 3.3; O−N, 3.4; N−N, 3.4. Waters belonging to different structures were considered equivalent if their interatomic distance was less than 0.5 Å.

ordered solvent molecules. An electron density difference peak was modeled as a water molecule if it was higher than 3.5σ, made contact with at least one potential hydrogen bond donor or acceptor within 2.4−3.4 Å and remained in the electron density (1σ, $2F_o-F_c$) after subsequent rounds of refinement. The solvent structure of the wild-type complex was not used to assist the placement of water molecules in the mutant structures. Table 1 shows data collection and refinement statistics for the V_L92A, V_L92F, V_L92H, V_L92S, and V_L92V complex structures. Statistics for the wild-type

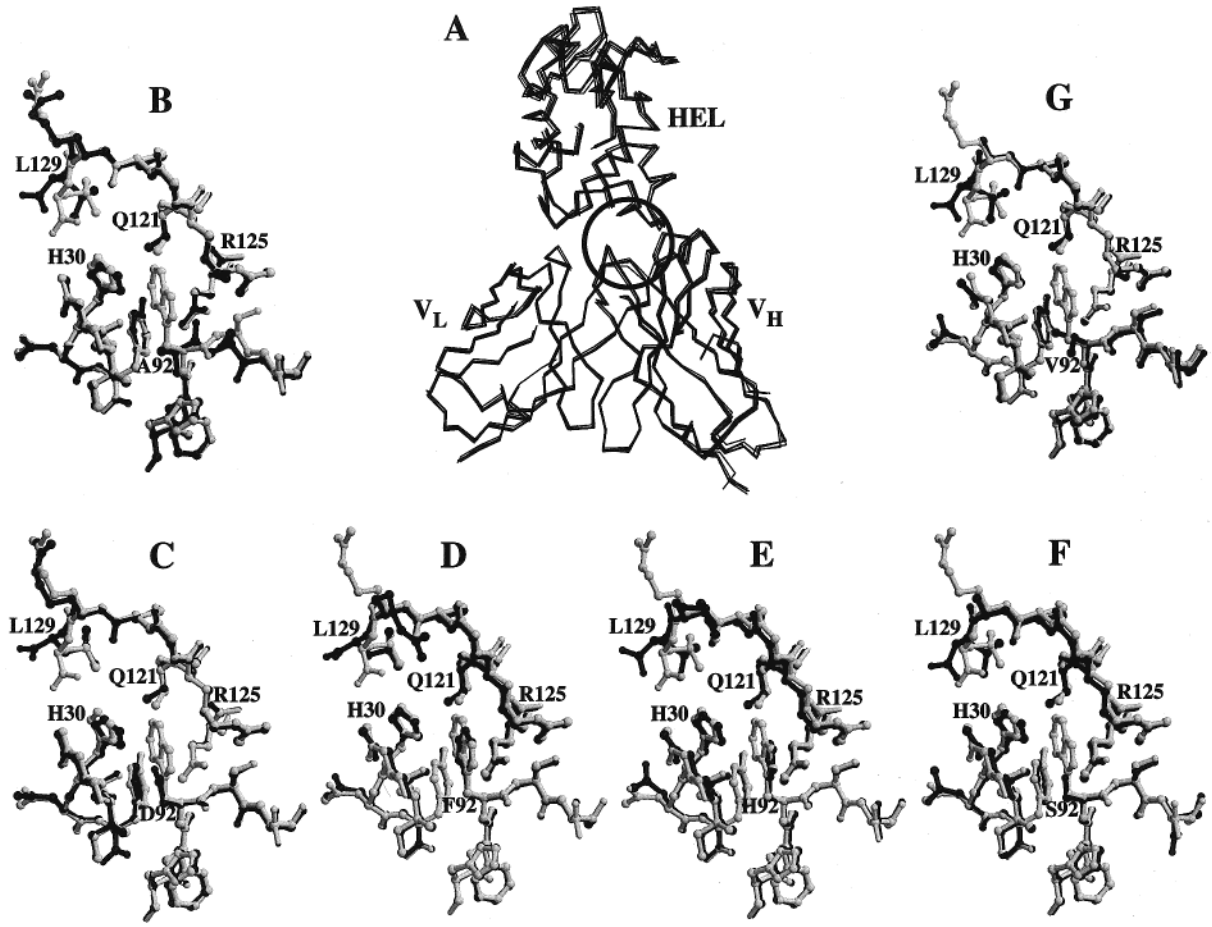

FIGURE 1: Superpositions of mutant and wild-type FvD1.3 V_L92-HEL complexes. (A) Superpositions of all Cα atoms from the FvD1.3 V_L92-HEL complex structures, including wild-type V_LW92, V_LW92A, V_LW92D, V_LW92H, V_LW92F, V_LW92S, and V_LW92V. The circle highlights the protein interface region around residue V_L92 that is presented in greater detail for each of the mutant complex structures superimposed onto the FvD1.3−HEL wild-type structure in panels B−G, where the wild-type structure is drawn in white and the mutant structures are drawn in black. (B) V_LW92A. (C) V_LW92D. (D) V_LW92F. (E) V_LW92H. (F) V_LW92S. (G) V_LW92V.

(*22*) and V_L92D mutant (*25*) complexes are reported elsewhere.

Calculation of Accessible Surface Areas. Changes in apolar, polar, and aggregate accessible surface areas were calculated using the programs AREAIMOL and DIFFAREA from the CCP4 suite of programs (*44*) with a probe radius of 1.4 Å. These programs calculate changes in accessible surface area upon complex formation according to the algorithm defined by Lee and Richards (*45*).

RESULTS AND DISCUSSION

Structures of Wild-Type and Mutant FvD1.3−HEL Complexes. The high resolution (1.8 Å) crystal structure of the FvD1.3−HEL complex has been reported previously (*22*). The binding interface is characterized by an extensive buried surface involving 16 HEL residues, 17 D1.3 residues, and 25 well-ordered water molecules, which mediate 17 hydrogen bonds and a large number of van der Waals interactions through main-chain, side-chain, and solvent network interactions. Alanine scanning mutagenesis studies in which amino acid residues residing in the binding interface were mutated to alanine, and the free energy of binding to HEL was measured (*23*) to show that such an extensive network of noncovalent bonding interactions is not necessary for D1.3−HEL complex formation. Instead, binding in the complex is largely dependent on a structurally smaller functional epitope in the D1.3 molecule that includes only residues V_LW92, V_HD100, and V_HY101. Further mutational analysis by double mutant cycles (*24*) has revealed significant coupling energies between HEL residue Q121 and D1.3 residues V_LW92 and V_LY32. The tryptophan residue at position V_L92 fills a sizable and predominantly hydrophobic pocket on the surface of HEL, characterized by extensive van der Waals interactions with HEL residues Q121, I124, and R125 as well as interactions through two water molecules to main-chain atoms of G126 and C127 (Table 2; Figure 3A). In the free D1.3 structure, 93 Å^2 of the surface area of residue V_LW92 is accessible to solvent, while upon complex formation with HEL, the accessible surface area of this residue is reduced to 17 Å^2 (*22*).

The three-dimensional structure of the D1.3 mutant V_LW92D complexed with HEL has been determined previously by X-ray crystallography to a resolution of 1.8 Å (*25*). The major structural change in this mutant complex as compared to the wild-type complex is a rearrangement of the water network at the D1.3−HEL interface where two water molecules occupy part of the space previously occupied by the tryptophan side chain (Figure 3C). All of the direct interactions between the V_L92 residue side chain and HEL are lost when this residue is mutated from tryptophan to aspartate (Table 2). Only two van der Waals interactions to HEL residue R125, now mediated through a water molecule,

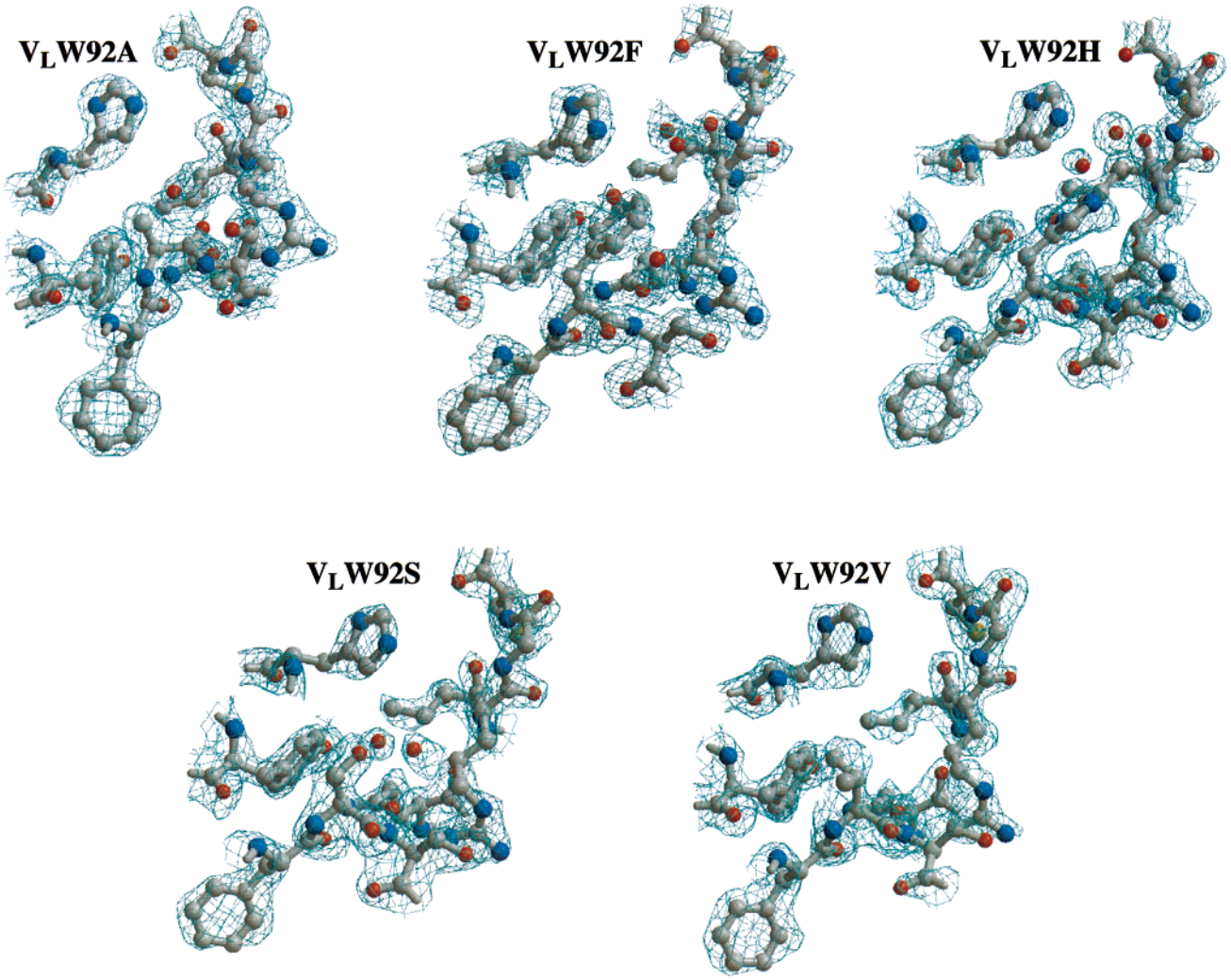

FIGURE 2: Simulated annealing omit electron density maps for the interface region around FvD1.3 position V_L92. Maps were calculated using CNS (*42*) where all atoms within a 9-Å sphere of residue V_L92 were omitted from the calculation. Map contours are at 1.2σ.

and the water-bridged interaction with the main chain of HEL G126 are retained in this mutant complex. Unlike the rearranged solvent network in the D1.3−HEL(D18A) complex that fully compensates energetically for the loss of one hydrogen bond and seven van der Waals interactions (*24*), the newly formed solvent network in the D1.3(V_LW92D)−HEL complex is associated with a reduction of the binding affinity by 100-fold ($\Delta\Delta G = 3.1$ kcal/mol) due presumably to loss of extensive hydrophobic and van der Waals packing interactions upon substitution of the tryptophan side chain.

To seek correlations between structural changes at the D1.3 V_L92 hot spot and changes in thermodynamic binding parameters, we have determined the crystal structures of five additional D1.3−HEL complexes in which D1.3 residue V_LW92 has been mutated to alanine, phenylalanine, histidine, serine, and valine. These mutations were chosen because they were expected to decrease the amount of buried surface area at this position by different amounts. The crystal structures of all of these complexes have been solved to a nominal resolution of at least 2.0 Å. As with other point mutants in the D1.3−HEL complex (*24*, *26*), the Cα atoms of the mutant complexes superimpose well onto the wild-type structure, with root-mean-square deviations ranging from 0.21 to 0.44 Å. As shown in Figure 1A, the largest main chain movement in the mutant complexes occurs in HEL on the side of the molecule opposite the epitope for D1.3. Close-up views of the region surrounding the mutation site of individual mutant complexes superimposed onto the wild-type complex (Figure 1B−G) show that the only significant atomic movements in this region occur at the HEL C-terminal residue L129, for which there is commonly poor side-chain density, and the main chain of D1.3(V_LW92A) in which a peptide flip occurs at the mutation site.

Simulated annealing omit maps for D1.3 and HEL residues and water molecules in the region surrounding the mutation site for the mutant D1.3−HEL complexes reported in this study are shown in Figure 2. The major structural change in these complexes, as in the V_LW92D−HEL complex, is the rearrangement of solvent at the D1.3−HEL interface, except in the case of V_LW92V−HEL in which no evidence was found for ordered water molecules in the cavity created by the tryptophan side-chain replacement. Table 2 lists the direct contacts made by residue V_L92 in the wild-type and mutant complexes with HEL residues and interface water molecules. It is evident that nearly all of the direct van der Waals interactions between D1.3 residue V_LW92 and HEL are lost upon mutation of the tryptophan. Only in the alanine mutant complex, in which a peptide flip at the mutated residue allows a direct interaction between the V_LA92 main-chain oxygen and the Cδ atom of HEL residue R125, is this not the case.

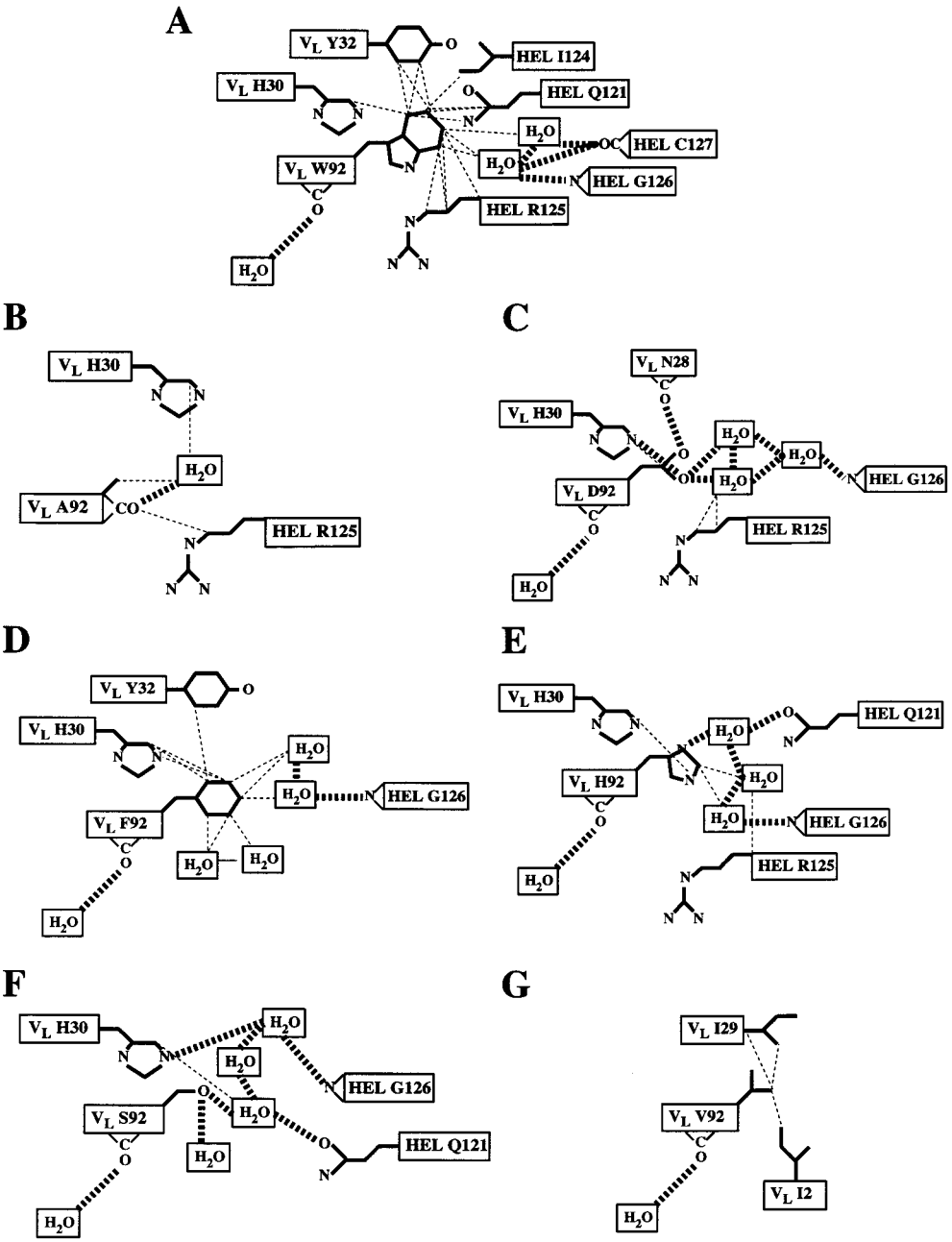

FIGURE 3: Schematic representations of the FvD1.3 V_L92-HEL wild-type and mutant complexes. Hydrogen bonding interactions are represented by thick dotted lines; van der Waals contacts are drawn as thin dotted lines. (A) Wild-type V_LW92. (B) V_LW92A. (C) V_LW92D. (D) V_LW92F. (E) V_LW92H. (F) V_LW92S. (G) V_LW92V.

The schematic diagrams in Figure 3 highlight that not only are the direct interactions of the wild-type complex predominantly lost in the mutant complexes but also that the rearranged solvent networks, which are quite extensive in some cases, do not necessarily mediate these interactions, nor are they generally replaced by newly formed water-mediated interactions. In fact, only in the histidine and serine mutant complexes is a new water-mediated interaction between the side chain of the mutated residue and the Oζ atom of HEL residue Q121 made (Figure 3; Table 2). Even when V_LW92 is replaced by a relatively bulky phenylalanine residue that makes contact with four water molecules, none of the interactions made by the tryptophan, except the water-mediated interaction with the main-chain nitrogen of HEL residue G126, remain. This nearly complete abolishment of the direct and indirect wild-type interactions between residue V_L92 and HEL in the mutant complexes is most likely the cause of the substantial loss of enthalpy of formation relative to wild-type observed for each of the mutant complexes, as discussed below.

Thermodynamic Properties of Association in the Wild-Type and Mutant FvD1.3−HEL Complexes. Because the affinity was too high to be reliably estimated by titration calorimetry, the interaction of wild-type FvD1.3 with HEL was measured by surface plasmon resonance under equilibrium binding conditions (data not shown), as previously described (*24*, *26*). The resulting association constant was used to determine the binding free energy. This value and the enthalpy of formation of the wild-type complex as measured by titration calorimetry were used to calculate the change in entropy upon association. In contrast, the affinities of all six mutant complexes were sufficiently low to be determined by titration

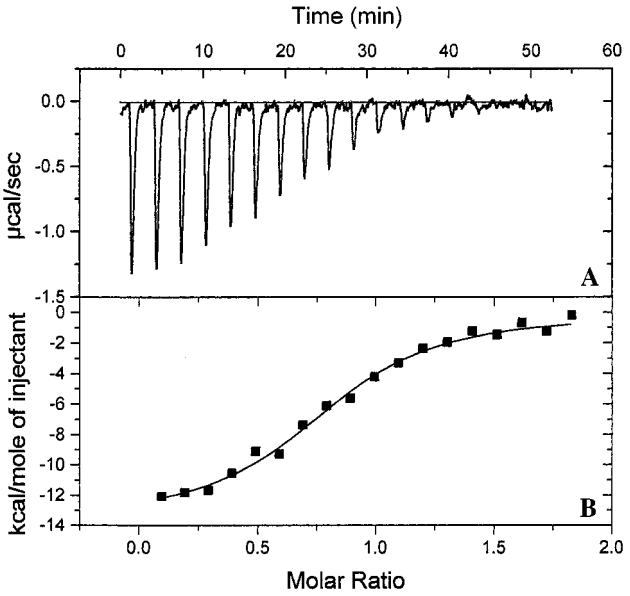

FIGURE 4: Calorimetric titration of HEL solution into solution of an FvD1.3 V_L92 mutant. The power released per addition of 10-μL aliquots of 0.5 mM HEL in PBS to 0.026 mM FvD1.3 V_LW92S at 24.0 °C as a function of run time is shown in panel A. The incremental binding enthalpy as a function of molar ratio, panel B, for the titration data presented in panel B. The solid curve is the result of a least-squares fit of the data to the Origin single-site binding model (*33*) to obtain values for K_b and ΔH_b.

calorimetry, as shown in Figure 4 for the binding of the V_LW92S mutant to HEL. The binding constant values obtained by both surface plasmon resonance and calorimetric techniques are consistent with one another as demonstrated by comparing these values for one of the mutants as measured using both techniques. The K_b value of the V_LW92A mutant reported in this study as measured by titration calorimetry ($3.3 \pm 1.0 \times 10^5$ M^{-1}) is in close agreement with the corresponding K_b value obtained using surface plasmon resonance ($2.5 \pm 0.8 \times 10^5$ M^{-1}), as reported previously by our laboratory (*24*).

The thermodynamic parameters for the interaction of wild-type D1.3 and the series of V_L92 mutants with HEL are listed in Table 3. The wild-type complex exhibits the highest association constant, $K_b = 5.0 \times 10^7$ M^{-1}. All of the mutations at residue V_L92 analyzed in this study resulted in a decrease in the binding affinity between D1.3 and HEL of 10−100-fold. As with the wild-type complex, the mutant D1.3 molecules all form complexes with HEL in an enthalpically driven process with an opposing entropic

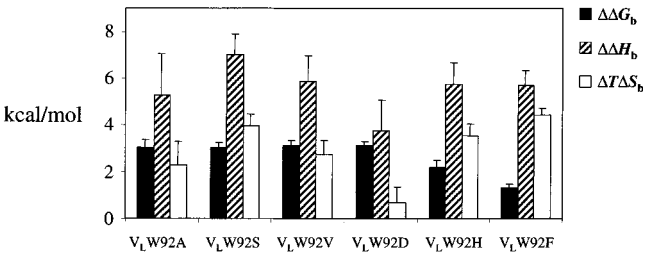

FIGURE 5: Changes in thermodynamic parameters for the FvD1.3 V_L92-HEL mutant complexes compared to wild-type. $\Delta\Delta G_b$ black bars; $\Delta\Delta H_b$ hatched bars; $\Delta(T\Delta S_b)$ white bars. The mutants are arranged in order of increasing side chain volume (V_LW92A to V_LW92F).

penalty that is significant yet smaller than in the wild-type complex. Each of the mutant complexes is marked by a reduction in the enthalpy of complex formation as compared to the wild-type, with $\Delta\Delta H_b$ values ranging from 3.8 to 7.0 kcal/mol, as shown in Figure 5, such that the decreases in binding enthalpy exceed the decreases in binding free energy. These unfavorable enthalpy changes probably arise, at least in part, from the loss of van der Waals contacts and disruption of the hydrogen-bonded interface solvent network (Figure 3; Table 2). For each mutant relative to wild-type, the loss of enthalpy is offset by a gain in entropy of the system. The values of $\Delta(T\Delta S_b)$ vary from 0.7 to 4.4 kcal/mol in the six mutant complexes. The variation in entropy values is even more striking when viewed as an energetic term that compensates for the loss of enthalpy upon binding of mutant D1.3 and HEL molecules, a phenomenon that has been noted previously in the D1.3−HEL system (*26*, *46*). For example, by mutating V_LW92 to a serine residue, there is an enthalpic loss of 7.0 kcal/mol relative to the wild-type complex. However, more than half of this unfavorable energy term, 4.0 kcal/mol, is compensated by a relative gain in entropy in the V_LW92S−HEL complex. The entropic compensation for the enthalpic loss in each mutant complex varies greatly depending on the particular mutation at residue V_L92. Surprisingly, for the mutant most similar to V_LW92S, replacement of the wild-type tryptophan residue with aspartate, an essentially negligible $\Delta(T\Delta S_b)$ was observed (*25*), and the difference in binding free energy for this mutant relative to wild-type results almost exclusively from the enthalpic loss during complex formation.

Entropic changes upon complex formation are defined by the summation of the conformational ($\Delta S_{conformation}$) and solvent ($\Delta S_{solvent}$) entropy terms, derived from atomic move-

Table 3: Thermodynamic Parameters for the Binding of Wild-Type and Mutant FvD1.3 to Hen Egg White Lysozyme

	V_LW92	V_LW92A	V_LW92D	V_LW92F	V_LW92H	V_LW92S	V_LW92V
temperature (°C)	24.0 ± 0.1	24.0 ± 0.1	24.0 ± 0.1	24.0 ± 0.1	24.0 ± 0.1	24.0 ± 0.1	24.0 ± 0.1
$-\Delta H_b$ (kcal/mol)	21.5 ± 0.4	16.3 ± 1.4	17.7 ± 0.9	15.8 ± 0.2	15.8 ± 0.5	14.5 ± 0.5	15.7 ± 0.7
K_b (M^{-1})	$5.0 \pm 0.8 \times 10^7$	$3.3 \pm 1.0 \times 10^5$	$2.6 \pm 0.5 \times 10^5$	$5.7 \pm 1.0 \times 10^6$	$1.2 \pm 0.4 \times 10^6$	$2.9 \pm 0.3 \times 10^5$	$2.5 \pm 0.4 \times 10^5$
$-\Delta G_b$ (kcal/mol)[a]	10.5 ± 0.1	7.5 ± 0.2	7.4 ± 0.1	9.2 ± 0.1	8.3 ± 0.2	7.4 ± 0.1	7.3 ± 0.1
$-T\Delta S_b$ (cal K^{-1} mol^{-1})	11.0 ± 0.2	8.7 ± 0.8	10.4 ± 0.5	6.6 ± 0.1	7.5 ± 0.3	7.1 ± 0.3	8.3 ± 0.4
$-T\Delta S_{conformation}$ (cal K^{-1} mol^{-1})	14.9 ± 0.2	12.2 ± 0.1	10.0 ± 0.1	10.7 ± 0.2	10.6 ± 0.2	8.1 ± 0.1	10.2± 0.1
$-T\Delta S_{solvent}$ (cal K^{-1} mol^{-1})	−3.9 ± 0.2	−1.8 ± 0.1	−1.3 ± 0.1	−4.1 ± 0.2	−3.1 ± 0.2	−1.0 ± 0.1	−1.9 ± 0.1
$\Delta\Delta ASA_{aggregate}$ (Å^2)[b]		143	102	40	69	108	110
$\Delta\Delta ASA_{apolar}$ (Å^2)[b]		115	104	25	60	99	99
$\Delta\Delta ASA_{polar}$ (Å^2)[b]		28	−2	15	9	11	11

[a] $\Delta G_b = \Delta H_b - T\Delta S_b = -RT \ln(K^b)$. [b] $\Delta\Delta ASA$ values calculated excluding fixed water molecules.

ments and the exclusion of bulk solvent, respectively. Thus, increases in solvent and protein motion in the mutant complexes relative to the wild-type complex could signify an increase in the entropy of the system. This should be indicated by the crystallographic temperature factors (*B*) of the mutated residue and the neighboring amino acids when the structures being compared crystallize isomorphously, which is the case for all of the D1.3−HEL complexes reported here. No significant changes in *B* factors, for the entire complex, the mutated residue, or residues and water molecules surrounding the mutation site, are seen when comparing the wild-type and mutant complexes (data not shown). In fact, the V_LW92F−HEL complex, which has the highest measured value of $\Delta(T\Delta S_b)$ in the series, has the lowest mean temperature factors for amino acid residues and solvent molecules inclusive of and surrounding the mutation site. These observations run counter to the expected correlation between *B* values and entropy changes and contrast with results obtained for mutations at certain other sites in the D1.3−HEL interface. For example, increases in the mobility of side chains in the vicinity of mutations were observed for the V_LY50S−HEL and V_HY32A−HEL complexes, which probably contribute to the measured gains in entropy relative to the wild-type complex (*26*). On the other hand, in common with the V_L92 series described here, no increases in temperature factors for atoms near the mutation site were noted for the V_LY101F−HEL complex that could account for the large observed $\Delta(T\Delta S_b)$ value (4.9 kcal/mol) (*26*). Alternatively, residue V_L92 (or its neighbors) may be significantly less mobile in the unliganded mutant FvD1.3 molecule than in the wild-type structure, such that the mobility of the unbound mutated residue is much closer to its mobility in the complex than in the case of the wild-type residue. Again, although this cannot be formally addressed in the absence of crystal structures of both free mutant and free wild-type antibodies, the available evidence does not support this explanation for entropy compensation. First, the mean *B* factor of residue V_LW92 in the unbound wild-type Fv is indistinguishable from that in the complex, indicating a lack of significant quenching of side-chain mobility upon complex formation, which would be entropically unfavorable for binding (*22*). Second, as noted above, no differences in *B* factors for residue V_L92 are evident when comparing mutant and wild-type complexes. Thus, significantly reduced quenching of side-chain mobility for V_L92 in the mutant complexes as compared to wild-type is unlikely. It may be that the common use of temperature factor values to explain either global or local changes in entropy is not always valid. Certainly, in the case of the FvD1.3−HEL mutant complexes, no obvious thermodynamic extrapolations can be made using crystallographic *B* factors. Recently, several NMR studies have investigated changes in localized side chain/backbone movement of protein residues involved in protein−protein interactions and the redistribution of side chain entropy throughout the complex (*47*, *48*). Similar site-specific measurements of entropy changes in the FvD1.3−HEL system by NMR may yield a better correlation with the thermodynamic data presented here than do the crystallographic temperature factors.

Changes in binding entropy may also result from differences in solvent structure between FvD1.3 in its free and HEL-bound states. Accordingly, larger increases in entropy should occur for those FvD1.3 molecules that order more water in their unbound form and release these solvent molecules upon being buried in the binding interface, as measured by their respective $\Delta S_{solvent}$ values. The exclusion of solvent molecules from apolar surfaces is the main component of the hydrophobic effect that provides the driving force for protein folding (*1*) and is thought to be essential for protein−protein associations (*2*−*6*). Calculation of the $\Delta S_{solvent}$ values for the V_L92 mutant series in the association between D1.3 and HEL bears out the importance of water exclusion in this molecular interaction. In the case of each D1.3 molecule, there exists a positive $\Delta S_{solvent}$ term that counteracts a negative and much larger $\Delta S_{conformation}$ term (Table 3). Not surprisingly, the $\Delta(T\Delta S_{solvent})$ terms for the V_L92 mutants are negative as the mutated side chains are each smaller than the wild-type tryptophan side chain and would be expected to exclude less water from the binding interface. Only in the case of the phenylalanine mutation at position V_L92 is there a positive $\Delta(T\Delta S_{solvent})$ value. Additionally, these changes in $T\Delta S_{solvent}$ are highly correlated with changes in the buried apolar accessible surface area upon mutation of V_LW92, as discussed below.

Estimation of the Hydrophobic Effect at Position V_L92 in the D1.3−HEL Interface. On the basis of free energies of transfer of small hydrophobic solutes including nonpolar amino acids, from water to hydrophobic solvents, values of 20−30 cal mol^{-1} Å^{-2} have been proposed for the hydrophobic effect (*7*−*11*). By taking into account solute−solvent size differences, Sharp et al. (*49*) arrived at a higher estimate of the interfacial free energy derived from solubility data of about 50 cal mol^{-1} Å^{-2}. For protein−protein complexes, Nicholls et al. (*50*) used a geometric model for the curvature dependence of the hydrophobic effect to identify two distinct contributions to binding: one from residues completely buried in the center of the interface and one from partially buried residues at the periphery. The effective hydrophobicity of central residues was estimated at about 60 cal mol^{-1} Å^{-2} and that of peripheral residues at about 40 cal mol^{-1} Å^{-2}. In this study, we have sought to further extend these analyses in order to quantify the hydrophobic effect at the interfaces of associating proteins. Here, we attempt to correlate the measured changes in thermodynamic parameters with changes in buried accessible surface areas (ΔASA) in the binding interface between D1.3 molecules mutated at position V_L92 and HEL relative to the wild-type interaction.

We utilized the Lee and Richards algorithm (*45*) to calculate changes in ASA upon complex formation, using a probe radius of 1.4 Å. It is essential to choose the appropriate accessible surfaces over which to calculate ΔASA. Because of the crystallographic isomorphism of the wild-type and mutant complex structures, calculation of ΔASA values for the entire binding interface was necessary only for the determination of ΔC_p and not for correlations with thermodynamic parameters. Due to systematic errors in the programs used to calculate ΔASA values, attempting to determine small changes in ASA caused by point mutations within the context of the entire interface reduces the accuracy of the measurements. Calculations of this type (data not shown) do closely parallel the results presented in the discussion below, although the correlations are not quite as strong. Due to local nonisomorphism in the V_LW92A mutant caused by a peptide flip of the bond between residues V_L92 and V_L93,

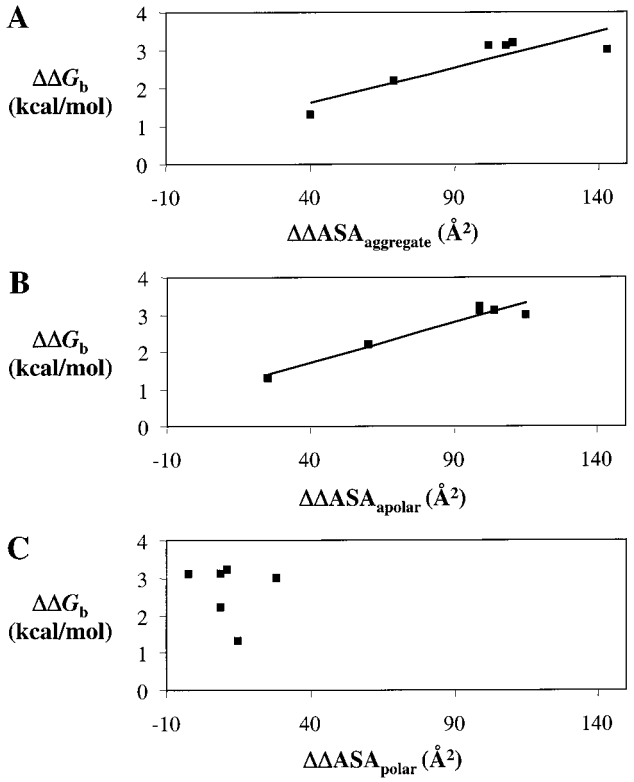

FIGURE 6: Correlations between $\Delta\Delta G_b$ and changes in aggregate (A), apolar (B), and polar (C) accessible surface areas between the FvD1.3−HEL wild-type and mutant complexes. The best-fit line from least-squares regression analysis between $\Delta\Delta G_b$ and the changes in $\Delta ASA_{aggregate}$ and ΔASA_{apolar} are drawn in panels A and B, respectively.

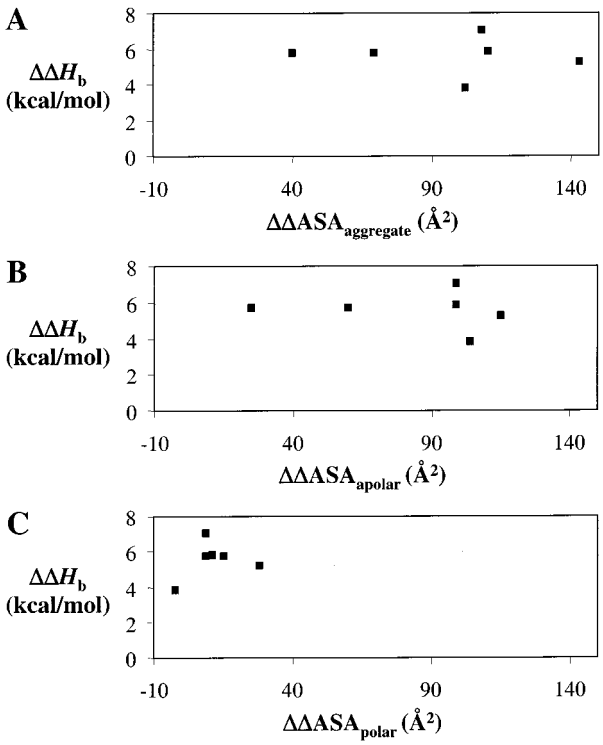

FIGURE 7: Correlations between $\Delta\Delta H_b$ and changes in aggregate (A), apolar (B), and polar (C) accessible surface areas between the FvD1.3−HEL wild-type and mutant complexes.

it would be inappropriate to calculate ΔASA for only the residue at position V_L92. Instead, we present data in the discussion below for which we have calculated ΔASA values for residues V_L91-V_L94. These amino acids constitute the loop of solvent-exposed residues (in the unbound D1.3 molecule) on which residue V_L92 is located. One further concern when calculating ΔASA values for macromolecular interfaces is how one deals with interface water molecules. In our ΔASA calculations for the VL92 mutant series, inclusion of crystallographically located waters affect only the polar component of the ΔASA values (data not shown). As is seen below, correlations between the thermodynamic parameters of binding and ΔASA are primarily limited to the apolar component of the surface area, and thus, the discussion below is by and large limited to ΔASA calculations made for the V_L91-V_L94 loop packing against HEL without interface water molecules.

Differences in the free energy of binding ($\Delta\Delta G_b$) and ΔASA upon complex formation ($\Delta\Delta ASA_{aggregate}$) between the V_L92 wild-type and mutant complexes are weakly correlated for the six V_L92 mutant complexes in this study (Figure 6A). Linear regression analysis for these six data points results in an R^2 value of 0.782. When the changes in ΔASA are deconvoluted into their apolar and polar components (Figure 6B,C), it becomes clear that $\Delta\Delta G_b$ is linearly dependent on the $\Delta\Delta ASA_{apolar}$ value ($R^2 = 0.937$). The slope of this line is 0.0214, corresponding to an effective hydrophobicity at position V_L92 of 21.4 cal mol^{-1} Å^{-2}. Conversely, $\Delta\Delta ASA_{polar}$ and $\Delta\Delta G_b$ reveal no correlation, showing why the correlation for $\Delta\Delta G_b$ is weaker with $\Delta\Delta ASA_{aggregate}$ than with $\Delta\Delta ASA_{apolar}$. When ΔΔASA values are calculated incorporating fixed water molecules in the binding interface, the correlation between $\Delta\Delta G_b$ and $\Delta\Delta ASA_{aggregate}$ becomes slightly stronger ($R^2 = 0.799$). This is likely due to a more accurate polar surface area for which a weak linear correlation exists ($R^2 = 0.753$) between $\Delta\Delta G_b$ and $\Delta\Delta ASA_{polar}$ (data not shown). Inclusion of fixed water molecules in the ΔΔASA calculations do not affect the $\Delta\Delta ASA_{apolar}$ values, and thus, the correlation between $\Delta\Delta ASA_{apolar}$ and $\Delta\Delta G_b$ is unaffected.

In contrast to the strong correlation between the loss of buried apolar accessible surface area at position V_L92 and the decrease in binding free energy, no correlations were observed between the aggregate, apolar, or polar changes in accessible surface area and changes in the binding enthalpy (Figure 7A−C). This suggests that measurements of ΔG_b may be preferable to those of ΔH_b for simple thermodynamic analysis of protein−protein interactions. A similar conclusion was reached in a calorimetric study of the interaction of barnase with barstar (*51*). In both cases, changes in ΔH_b are large and erratic as compared to changes in ΔG_b. Thus, results from two independent systems do not support the argument that enthalpy measurements are a theoretically more sound means of assigning energies to specific residue−residue interactions than free energy measurements (*52*).

In protein folding, the driving force of the hydrophobic effect is the exclusion of water molecules in the tightly packed apolar protein core (*1*). It follows that the exclusion of solvent is likely the predominant factor in hydrophobic interactions between protein residues at the binding interface, which should be observed in changes in the solvent portion of the entropy term. For the six V_L92 mutant complexes, there is a clear correlation between $\Delta\Delta ASA_{apolar}$ and $\Delta(T\Delta S_{solvent})$ ($R^2 = 0.909$, Figure 8B). As is the case for

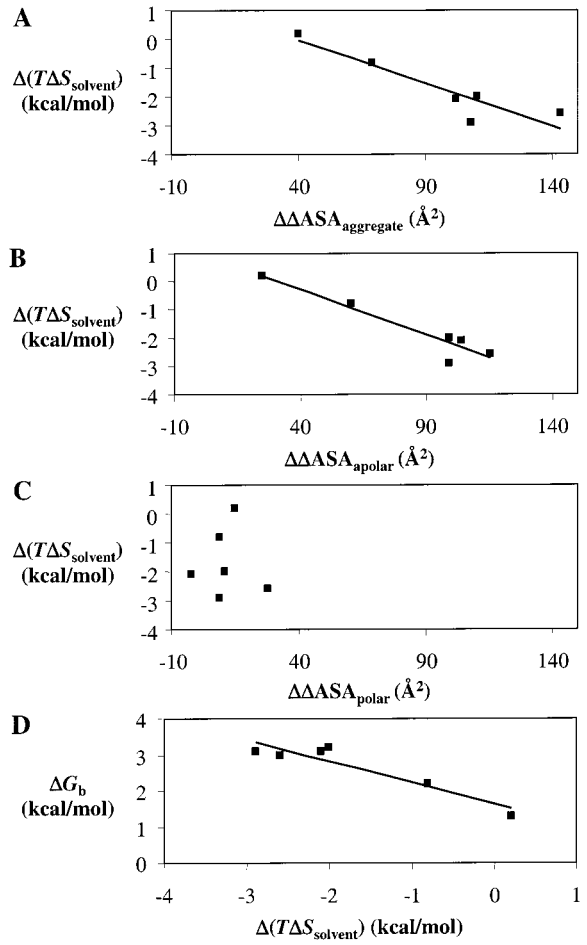

FIGURE 8: Correlations between $\Delta(T\Delta S_{solvent})$ and changes in aggregate (A), apolar (B), and polar (C) accessible surface areas between the FvD1.3−HEL wild-type and mutant complexes. The best-fit line from least-squares regression analysis between $\Delta(T\Delta S_{solvent})$ and the changes in $\Delta ASA_{aggregate}$ and ΔASA_{apolar} are drawn in panels A and B, respectively. (D) Correlation between $\Delta\Delta G_b$ and $\Delta(T\Delta S_{solvent})$ for the V_L92 mutant series, including the best-fit line from least-squares regression analysis.

$\Delta\Delta G_b$, $\Delta\Delta ASA_{polar}$ does not correlate to $\Delta(T\Delta S_{solvent})$ (Figure 8C) and, thus, $\Delta(T\Delta S_{solvent})$ is more poorly correlated to $\Delta\Delta ASA_{aggregate}$ ($R^2 = 0.844$, Figure 8A) than to $\Delta\Delta ASA_{apolar}$. Because $\Delta\Delta G_b$ and $\Delta(T\Delta S_{solvent})$ are both linearly correlated to $\Delta\Delta ASA_{apolar}$, they also must be linearly correlated to one another ($R^2 = 0.875$, Figure 8D). Importantly, the slope of the line defined by the $\Delta\Delta G_b$ and $\Delta(T\Delta S_{solvent})$ values of the six V_L92 mutant complexes is −1.46. In order for all binding free energy differences to be caused by changes in $T\Delta S_{solvent}$ between the wild-type and mutant complexes, the slope of this line would need to be one. Instead, factors other than changes in the solvent entropy, for which we cannot account in this study, contribute to changes in the binding free energy. The solvent portion of the entropy term, however, is the predominant factor affecting changes in ΔG_b for the V_L92 mutant complexes.

The decrease in binding free energy and the increase in solvent entropy associated with the loss of buried apolar surface area (Figures 6B and 8B) must be the consequence of reduced hydrophobic interactions at the complex interface and/or loss of van der Waals contacts, since neither wild-type nor mutated residues at position V_L92 form direct hydrogen bonds to HEL. We believe that our measured value of 21 cal mol^{-1} Å^{-2} for the contribution of the buried apolar unit area to the decrease in free energy is predominantly attributable to the hydrophobic effect, with only a relatively small contribution from van der Waals interactions. As shown in Table 2 and Figure 3, residues V_LA92, V_LD92, V_LS92, and V_LV92 make a variable number of direct or water-mediated contacts with HEL residues Q121, R125, or G126 with solvent networks linking the mutated residue to HEL present in the V_LA92, V_LD92, and V_LS92 complexes but not in the V_LV92 complex. Nevertheless, despite these differences in packing interactions, all four mutations, which are characterized by very similar decreases in buried apolar surface area (99−115 Å^2), result in nearly identical losses in binding free energy ($\Delta\Delta G_b$ = 7.3−7.5 kcal/mol). In addition, as discussed in the next section, the energetic contribution of V_LW92 to complex stabilization appears to depend much more on the chemical nature of the van der Waals contacts made by this residue than on their absolute number.

Our figure of 21 cal mol^{-1} Å^{-2} for the effective hydrophobicity at the V_L92 mutation site is comparable to estimates of the magnitude of the hydrophobic effect derived from classical hydrocarbon solubility models (*7*−*11*). Notably, this value is lower than estimates of the interfacial free energy for protein−protein interactions (*49*, *50*). It may be that partially solvent-exposed residues in protein−protein interfaces, such as those at position V_L92, are energetically more comparable to the transfer of small hydrophobic solutes from aqueous to apolar solvents because there is no extra energetic cost of cavity formation, as for those residues that comprise the hydrophobic cores of proteins (*12*−*19*). It is possible then that a similar structural and thermodynamic analysis of a hot spot residue in the D1.3−HEL interface that is completely buried in the interface, such as at position V_H101, will have a larger effective hydrophobicity that is more comparable to protein core residues.

Dependence of the Hydrophobic Effect on Local Environment. Although the significance of the hydrophobic effect in protein−protein associations is generally recognized, the quantitative importance of hydrophobic effects at individual sites in protein−protein interfaces has yet to be established. Dall'Acqua et al. (*23*) have compared the binding energetics of D1.3 to both HEL and the anti-D1.3 antibody E5.2 by alanine scanning mutagenesis. HEL and E5.2 share overlapping structural epitopes on the D1.3 surface (*53*) but differ greatly in their functional epitopes. Whereas only a small subset (3 of 13) of the D1.3 residues in the interface with HEL are energetically important for association, most (12 of 15) of the D1.3 residues in the interface with E5.2 make significant contributions to binding ($\Delta G_{mutant} - \Delta G_{wild-type} > 1.0$ kcal/mol). No general correlation was observed between the energetic importance of individual D1.3 residues to binding and the buried surface area of these residues in the D1.3−HEL and D1.3−E5.2 complexes (*24*). Significantly, there are two tryptophan residues common to the binding interface of both complexes, D1.3 V_LW92 and V_HW52. These have approximately equal buried surface areas in the D1.3−HEL and D1.3−E5.2 structures (*22*, *53*). However, V_LW92 acts as a hot spot in the D1.3−HEL complex ($\Delta\Delta G_{D1.3(VLW92A)-HEL}$ = 3.3 kcal/mol) but has little effect on the binding of D1.3 to E5.2 ($\Delta\Delta G_{D1.3(VLW92A)-E5.2}$ = 0.9 kcal/mol) (*24*). Conversely, V_HW52 contributes

insignificantly to the association of D1.3 to HEL ($\Delta\Delta G_{D1.3(VHW52A)-HEL} = 0.4$ kcal/mol) but plays an important energetic role in the D1.3−E5.2 complex ($\Delta\Delta G_{D1.3(VHW52A)-E5.2} = 4.2$ kcal/mol) (*23*). As the structures of D1.3 residues VLW92 and VHW52 in the unbound state are equivalent whether they are to bind HEL or E5.2 by definition, the reason that they are functionally dissimilar in the D1.3−HEL and D1.3−E5.2 complexes is most likely due to the local environments of the ligands against which the tryptophan residues are packed. Indeed, an analysis of the atomic interactions made by D1.3 residues V_LW92 and V_HW52 with HEL and E5.2 reveals that the two hot spots (V_LW92−HEL and V_HW52−E5.2) are dominated by carbon−carbon interactions (7 C−C, 1 C−N and 13 C−C, 2 C−O, 1 C−N, respectively), whereas the two energetically unimportant interactions (V_LW92−E5.2 and V_HW52−HEL) are composed of more of a mixture noncovalent interactions (3 C−C, 2 C−O, 3 C−N, 1 O−N and 6 C−C, 3 C−O, 2 C−N, respectively).

Differences in the buried apolar ASA of these two residues when bound to each ligand help to elucidate the role that the local binding environment plays in the thermodynamics of these protein−protein associations. In the D1.3−HEL complex, residue V_LW92 buries an apolar ΔASA of −147 Å^2, while residue V_HW52 buries −122 Å^2. The difference in buried apolar Δ*A*SA of 25 Å^2 corresponds to a free energy change of 1.4 kcal/mol, according to the correlation between $\Delta\Delta G_b$ and $\Delta\Delta ASA_{apolar}$ defined above (Figure 6A). This value, which we have termed $\Delta\Delta G_{environment}$, represents the estimated change in binding free energy that can be attributed to the hydrophobic differences in the binding surfaces encountered by the two tryptophan residues. Furthermore, one can estimate that the change in ΔG_b for a mutation of residue V_HW52 to alanine, if it were to pack against an environment that is structurally and chemically similar to the HEL binding interface for residue V_LW92, to be 2.3 kcal/mol; that is, the sum of $\Delta\Delta G_{D1.3(VLW52A)-HEL}$ and $\Delta\Delta G_{environment}$. Although this is not equivalent to the $\Delta\Delta G_{D1.3(VLW92A)-HEL}$ value of 3.3 kcal/mol, it is within the energetic range that defines a residue as a hot spot in binding. Analogously, the difference in buried apolar ASA for tryptophan residues at positions V_L92 and V_H52 in the D1.3−E5.2 complex is 98 Å^2, corresponding to a $\Delta\Delta G_{environment}$ of 3.0 kcal/mol. The free energy change for a V_LW92A mutation interacting with an environment similar to the E5.2 binding site for V_HW52 is estimated to be 3.4 kcal/mol. Again, although this value is not equivalent to that of $\Delta\Delta G_{D1.3(VHW52A)-E5.2}$, it could clearly be defined as a hot spot in binding. This analysis provides insight into the molecular interaction requirements of tryptophan residues to act as hot spots in protein−protein associations.

It is likely that these packing requirements hold true in other protein complexes. In the complex of human growth hormone with its receptor, a central contiguous core of hydrophobic residues confers the majority of binding energy to the complex (*54*−*56*). As in the D1.3 complexes with HEL and E5.2, no overall correlation was observed between the relative contribution of individual residues to the binding energetics and the buried surface area of these residues in the hormone−receptor complex. However, mutation of two tryptophans (W104 and W169) on the receptor side of the interface results in the greatest losses of binding free energy. Significantly, these hot spot tryptophans pack tightly against a hydrophobic surface on the hormone molecule composed of nonpolar residues and the alkyl portions of charged residues (*57*), much like the D1.3 hot spot tryptophans V_LW92 and V_HW52 do in complex with HEL and E5.2, respectively.

The above discussion underscores the importance of local environment in determining the contribution of individual residues to stabilizing protein−protein complexes. That is, not only must one consider the hydrophobicity of the residue itself but also that of the surface against which it packs. Unlike the organic solvents used in model experiments to measure free energies of transfer of nonpolar amino acids from water to hydrophobic environments (*7*−*11*), protein surfaces exhibit considerable chemical heterogeneity, such that buried surface area and location in the interface (i.e., central or peripheral) are by themselves insufficient indicators of a particular residue's importance in binding; consideration must also be given to its microenvironment in the complex. For this reason, our value of 21 cal mol^{-1} Å^{-2} for the effective hydrophobic energy at the V_L92 mutation site in the D1.3−HEL complex, although probably applicable to other sites in which hyrdophobic residues pack against predominantly hydrophobic surfaces, may be considerably less at sites where such residues are buried in more polar environments (e.g., D1.3 V_LW92 in the D1.3−E5.2 complex).

CONCLUSIONS

We have shown that for a single tryptophan hot spot, V_LW92 in the FvD1.3−HEL complex, changes in free energy of binding are directly correlated to changes in buried apolar surface area upon mutation to residues with smaller side chains. The effective hydrophobicity at this site is calculated to be 21 cal mol^{-1} Å^{-2} and is in good agreement with transfer free energy values for small hydrophobic solutes (*7*−*11*). Furthermore, the slope of the linear dependence of $\Delta\Delta G_b$ on changes in the solvent component of the entropy term, $\Delta(T\Delta S_{solvent})$, approaches unity, meaning that the freeing of bulk solvent from this site in the interface upon association is the predominant factor affecting the affinity of this complex.

Analysis of a limited number of tryptophan residues that reside in the binding interface of protein−protein complexes and act either as hot spots in binding or are thermodynamically unimportant in complex formation leads us to propose that tryptophan residues in protein−protein interfaces may be categorized as belonging to the functional epitope or not according to the polarity of the environment against which they pack. This may help in predicting the energetic importance of interface residues without such exhaustive mutational studies as presented here for position V_L92 in the D1.3−HEL complex.

ACKNOWLEDGMENT

We thank the reviewers for thorough reading of and constructive comments on the manuscript. E.J.S. is supported as a postdoctoral fellow by the Arthritis Foundation.

REFERENCES

1. Dill, K. A. (1990) *Biochemistry 29*, 7133−7155.
2. Chothia, C., and Janin, J. (1975) *Nature 256*, 705−708.

3. Janin, J., and Chothia, C. (1990) *J. Biol. Chem. 265*, 16027−16030.
4. Jones, S., and Thornton, J. M. (1996) *Proc. Natl. Acad. Sci. U.S.A. 93*, 13−20.
5. Bogan, A. A., and Thorn, K. S. (1998) *J. Mol. Biol. 280*, 1−9.
6. Lo Conte, L., Chothia, C., and Janin, J. (1999) *J. Mol. Biol. 285*, 2177−2198.
7. Chothia, C. (1976) *J. Mol. Biol. 105*, 1−14.
8. Reynolds, J. A., Gilbert, D. B., and Tanford, C. (1977) *Proc. Natl. Acad. Sci. U.S.A. 74*, 2925−2929.
9. Hermann, R. B. (1977) *Proc. Natl. Acad. Sci. U.S.A. 74*, 4144−4148.
10. Eisenberg, D., and McLachlan (1986) *Nature 319*, 199−203.
11. Ooi, T., Oobatake, M., Nemethy, G., and Sheraga, H. A. (1987) *Proc. Natl. Acad. Sci. U.S.A. 84*, 3086−3090.
12. Kellis, J. T., Jr., Nyberg, K., and Fersht, A. R. (1989) *Biochemistry 28*, 4914−4922.
13. Shortle, D., Stites, W. E., and Meeker, A. K. (1990) *Biochemistry 29*, 8033−8041.
14. Yutani, K., Ogasahara, K., Tsujiya, T., and Sugino, Y. (1987) *Proc. Natl. Acad. Sci. U.S.A. 84*, 4441−4444.
15. Matsumura, M., Becktel, W. J., and Matthews, B. W. (1988) *Nature 334*, 406−410.
16. Eriksson, A. E., Baase, W. A., Zhang, X.-J., Heinz, D. W., Blaber, M., Baldwin, E. P., and Matthews, B. W. (1992) *Science 255*, 178−183.
17. Takano, K., Ogasahara, Kaneda, H., Yamagata, Y., Fujii, S., Kanaya, E., Kikuchi, M., Oobatake, M., and Yutani, K. (1995) *J. Mol. Biol. 254*, 62−76.
18. Takano, Y., Yamagata, Y., Fujii, S., and Yutani, K. (1997) *Biochemistry 36*, 688−698.
19. Xu, J., Baase, W. A., Baldwin, E., and Matthews, B. W. (1998) *Protein Sci. 7*, 158−177.
20. Buckle, A. M., Henrick, K., and Fersht, A. R. (1993) *J. Mol. Biol. 234*, 847−860.
21. Buckle, A. M., Cramer, P., and Fersht, A. R. (1996) *Biochemistry 35*, 4298−4305.
22. Bhat, T. N., Bentley, G. A., Boulot, G., Greene, M. I., Tello, D., Dall'Acqua, W., Souchon, H., Schwarz, F. P., Mariuzza, R. A., and Poljak, R. J. (1994) *Proc. Natl. Acad. Sci. U.S.A. 91*, 1089−1093.
23. Dall'Acqua, W., Goldman, E. R., Eisenstein, E., and Mariuzza, R. A. (1996) *Biochemistry 35*, 9667−9676.
24. Dall'Acqua, W., Goldman, E. R., Lin, W., Teng, C., Tsuchiya, D., Li, H., Ysern, X., Braden, B. C., Li, Y., Smith-Gill, S. J., and Mariuzza, R. A. (1998) *Biochemistry 37*, 7981−7991.
25. Ysern, X., Fields, B. A., Bhat, T. N., Goldbaum, F. A., Dall'Acqua, W., Schwarz, F. P., Poljak, R. J., and Mariuzza, R. A. (1994) *J. Mol. Biol. 238*, 496−500.
26. Fields, B. A., Goldbaum, F. A., Dall'Acqua, W, Malchiodi, E. L., Cauerhff, A., Schwarz, F. P., Ysern, X, Poljak, R. J., and Mariuzza, R. A. (1996) *Biochemistry 35*, 15494−15503.
27. Mariuzza, R. A., Jankovic, D. Lj., Boulot, G., Amit, A. G., Saludjian, P., Le Guern, A., Mazie, J.-C., and Poljak, R. J. (1984) *J. Mol. Biol. 170*, 1055−1058.
28. Ruther, U., Koenen, M., Otto, K., and Muller-Hill, B. (1981) *Nucleic Acids Res. 9*, 4087−4098.
29. Ward, E. S., Gussow, D., Griffiths, A. D., Jones, P. T., and Winter, G. (1989) *Nature 341*, 544−546.
30. Tartof, K. D., and Hobbs, C. A. (1987*) Bethesda Res. Lab. Focus 9*, 12.
31. Goldbaum, F. A., Fields, B. A., Cauerhff, A., Ysern, X., Poljak, R. J., and Mariuzza, R. A. (1994) *J. Mol. Biol. 241*, 739−743.
32. Boulot, G., Eisele, J. L., Bentley, G. A., Bhat, T. N., Ward, E. S., Winter, G., and Poljak, R. J. (1990) *J. Mol. Biol. 213*, 617−619.
33. Wiseman, T., Williston, S., Brandts, J. F., and Lin, L. N. (1989) *Anal. Biochem. 179*, 131−137.
34. Schwarz, F. P., Puri, K. D., Bhat, R. G., and Surolia, A. (1993) *J. Biol. Chem. 268*, 7668−7677.
35. Luque, I., Mayorga, O. L., and Freire, E. (1996) *Biochemistry 35*, 13681−13688.
36. Gomez, J., Hilser, J. V., Xie, D., and Freire, E. (1995) *Proteins: Struct., Funct., Genet. 22*, 404−412.
37. Murphy, K. P., Bhakuni, V., Xie, D., and Freire, E. (1992) *J. Mol. Biol. 227*, 293−306.
38. Howard, A. J., Gilliland, G. L., Finzel, B. C., Poulos, T. L., Ohlendorf, D. H., and Salemme, F. R. (1987) *J. Appl. Crystallogr. 20*, 383−387.
39. Otwinowski, Z., and Minor, W. (1997) *Methods Enzymol. 276*, 307−326.
40. Brünger, A. T. (1992) *X-PLOR Version 3.1. A System for X-ray Crystallography and NMR*, Yale University Press, New Haven and London.
41. Navaza, J. (1994) *Acta Crystallogr. A50*, 157−163.
42. Brünger, A. T., Adams, P. D., Clore, G. M., DeLano, W. L., Gros, P., Grosse-Kunstleve, R. W., Jiang, J.-S., Kuszewski, J., Nilges, M., Pannu, N. S., Read, R. J., Rice, L. M., Simonson, T., and Warren, G. L. (1998) *Acta Crystallogr. D54*, 905−921.
43. Jones, T. A., Zou, J. Y., Cowan, S. W., and Kjeldgaard, M. (1991) *Acta Crystallogr. A47*, 110−119.
44. Collaborative Computational Project No. 4. (1994) *Acta Crystallogr. D50*, 760−763.
45. Lee, B., and Richards, F. M. (1971) *J. Mol. Biol. 55*, 379−400.
46. Braden, B. C., Goldman, E. R., Mariuzza, R. A., and Poljak, R. J. (1998) *Immunol. Rev. 163*, 45−57.
47. Feher, V. A., and Cavanagh, J. (1999) *Nature 400*, 289−293.
48. Lee, A. L., Kinnear, S. A., and Wand, A. J. (2000) *Nature Struct. Biol. 7*, 72−77.
49. Sharp, K. A., Nicholls, A., Fine, R. F., and Honig, B. (1991) *Science 252*, 106−109.
50. Nicholls, A., Sharp, K. A., and Honig, B. (1991) *Proteins: Struct. Funct. Genet. 11*, 281−296.
51. Frisch, C., Schreiber, G., Johnson, C. M., and Fersht, A. R. (1997) *J. Mol. Biol. 267*, 696−706.
52. Mark, A. E., and van Gunsteren, W. F. (1994) *J. Mol. Biol. 240*, 167−176.
53. Fields, B. A., Goldbaum, F. A., Ysern, X., Poljak, R. J., and Mariuzza, R. A. (1995) *Nature 374*, 739−742.
54. Cunningham, B. C., and Wells, J. A. (1993) *J. Mol. Biol. 234*, 554−563.
55. Clackson, T., and Wells, J. A. (1995*) Science 267*, 383−386.
56. Wells, J. A. (1996) *Proc. Natl. Acad. Sci. U.S.A. 93*, 1−6.
57. de Vos, A. M., Ultsch, M., and Kossiakoff, A. A. (1992) *Science 255*, 306−312.

BI000704L